Assessment of GHRSST and OISST Datasets in Identification of Marine Heat-Waves and Heat-Spikes

Hitesh Gupta and Sourav Sil, *Member, IEEE*

***Abstract*— This study assesses the performance of two satellite-derived products, viz. Group for High-Resolution Sea-Surface Temperature (GHRSST) and Optimum Interpolation Sea-Surface Temperature (OISST), in detecting the Marine Heat-Waves (MHWs) and Marine Heat-Spikes (MHSs) after a detailed validation with in situ instruments in the Bay of Bengal (BoB). A significantly good correlation and low Root Mean Square Error (RMSE) between GHRSST (OISST) and the Research Moored Array for African-Asian-Australian Monsoon Analysis and Prediction buoy at 15°N and 90°E (RM15) were found to be 0.97 (0.96) and 0.30 (0.35)°C, respectively. In comparison with three near-coast Wave-Rider-Buoys (WRBs), GHRSST (OISST) shows limited ability to reproduce daily temperature variability with RMSEs ranging from 0.61 °C to 1.07 °C (0.51 °C–1.08 °C), respectively. GHRSST captures signals below 1–2 month periodicity better than OISST, however, both products efficiently capture low-frequency variability (> 4 months). Finally, regarding the number of MHW counts and duration, the GHRSST (36 and 382 days) and OISST (33 and 294 days) overestimate these quantities with respect to RM15 (25 and 287 days). This results in RM15 having a higher duration per MHW event (11.48 days) than GHRSST (10.61 days) and OISST (8.91 days). GHRSST exhibited its highest counts (duration) of 7 (82 days) during 2020 (2010), whereas RM15 showed only 3 (55 days) counts (duration) during 2020 (2010). Moreover, the mean daily intensities from satellite-derived SSTs (0.86 °C) are comparable to RM15 (0.87 °C). Therefore, our study suggests that the satellite-derived SSTs are suitable to capture MHW characteristics in the open-ocean region of the BoB, but their use in the coastal regions should be judiciously done.**

***Index Terms*— Group for High-Resolution Sea-Surface Temperature (GHRSST), Marine Heat-Spikes (MHS), Marine Heat-Waves (MHW), Optimum Interpolation Sea-Surface Temperature (OISST), Sea-Surface Temperature (SST), wavelet analysis.**

I. Introduction

MOST of the heat transfer occurring at the air-sea interface are the manifestation of variability in Sea-Surface Temperature (SST) [1]. SST also defines the stability of the ocean surface by modulating its stratification, affecting the biological productivity of the ocean [2]. Moreover, SST helps in defining the coastal upwelling zones [3], [4]. Hence, accurate global SST data, whether from satellite observations or in situ measurements, is vital for understanding physical processes, monitoring climate change, and their assessment.

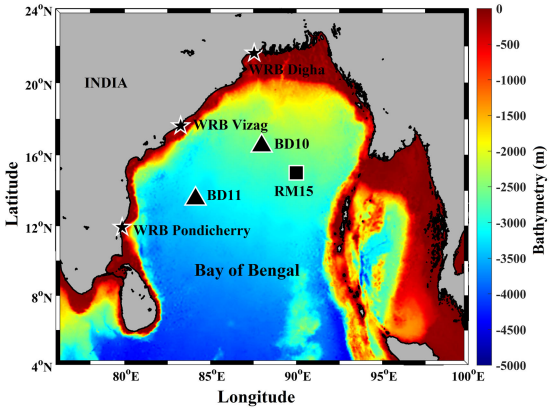

Fig. 1. Map of the BoB with marked locations of RM15 (square), WRBs (star), and OMNI Buoys (triangle). Colormap represents bathymetry in meters.

The Indian Ocean (IO), specifically the Bay of Bengal (BoB), harbors the Indian summer monsoon and cyclones, which are majorly modulated by local SST [5]. It was found that the episodes of anomalously high SST (higher than 90th percentile threshold), regarded as Marine Heat-Waves (MHWs) [6], modulates monsoon characteristics over the Indian mainland [7] and cyclonic activity over the BoB [8]. These MHWs are found to be linked to major climatic modes over the IO [7], [9]. MHWs are the global warming response of oceans and have major implications on climate change [10]. Therefore, to detect MHWs or Marine Heat-Spikes (MHSs) [6], and to understand its impact as an ocean stressor, accurate and precise measurements of SST is required. Along with accurate data, high spatio-temporal resolution is essential to understand the response of MHWs to various spatial-scale processes and its correspondence to the ocean-current system giving a decent idea of the spatial structures of MHWs.

In the era of satellite-based observations, SST measurements are taken in the form of brightness temperature which is then converted to actual temperature using various algorithms [11]. To reduce errors or biases, this data is generally objectively analyzed and optimally interpolated. Examples of such products are the Optimally Interpolated SST (OISST) and Group for High-Resolution SST (GHRSST) which are widely used over the global oceans [12], [13]. These satellite products have been extensively utilized to detect and understand the

Manuscript received 1 December 2023; revised 22 January 2024; accepted 1 February 2024. Date of publication 8 February 2024; date of current version 16 February 2024. *(Corresponding author: Sourav Sil.)*

The authors are with the School of Earth, Ocean, and Climate Sciences, Indian Institute of Technology Bhubaneswar, Odisha 752050, India (e-mail: hg13@iitbbs.ac.in; souravsil@iitbbs.ac.in).

Digital Object Identifier 10.1109/LGRS.2024.3362474

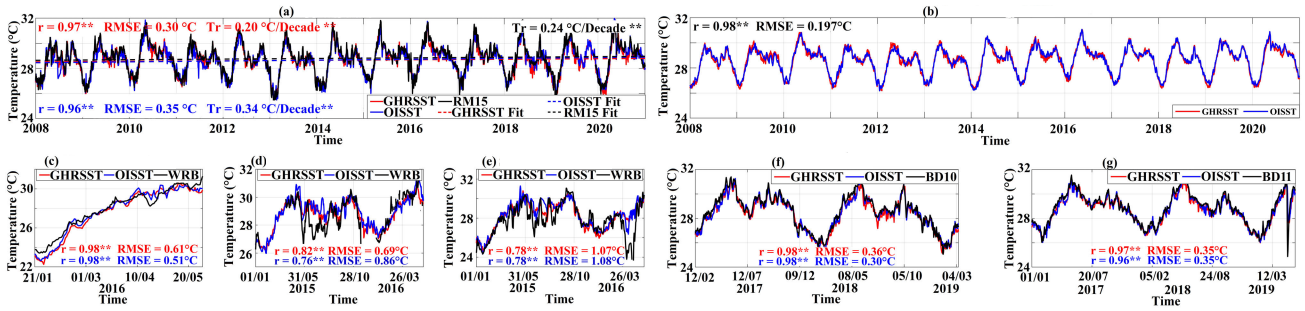

Fig. 2. Timeseries of GHRSST (red) and OISST (blue) against in situ (black). (a) RM15, (c) WRBD, (d) WRBP, (e) WRBV, (f) BD10, and (g) BD11. (a) Dashed red, blue, and black lines represent trends (Tr) with values written in the same color. In (a) and (c)–(g) correlation coefficient values represented by "r" and RMSE between GHRSST and in situ are given in red colored text, whereas blue color is used for OISST and in situ. (b) Represents the area-averaged timeseries of GHRSST and OISST over the BoB, with correlation and RMSE written in black-colored text. "**" against the values of r and Tr indicates more than 99% significance.

signatures of the MHWs over different regions of the world [14], [15], including the BoB [7], [9]. Gupta et al. [9] found a good correlation between GHRSST and OISST for the daily intensity of MHWs. However, the studies have not made objective comparisons of the suitability of these satellite products in MHW analysis with respect to in situ observations. Hence, herein we aim to assess the suitability of the GHRSST and OISST in identifying MHWs and MHSs, highlighting the strengths and weaknesses, in comparison to an in situ measurement. A precursor of this comparative analysis is a rigorous validation of the satellite-based SSTs against various in situ observations.

II. Data and Methodology

A. Data

The daily GHRSST and OISST datasets for the region of BoB (period: 2008–2020) are distributed by the Physical Oceanography Distributed Active Archive Center (https://podaac.jpl.nasa.gov/) and Physical Science Laboratory (https://psl.noaa.gov/data/gridded/). Daily SST data at Research Moored Array for African-Asian-Australian Monsoon Analysis and Prediction buoy present at 15°N and 90°E (RM15) [16], for the period of 2008–2020, are obtained from https://www.pmel.noaa.gov/tao/drupal/disdel/. 30-min SST data of Wave-Rider-Buoy (WRB) at Digha (WRBD), Pondicherry (WRBP), and Vizag (WRBV) are acquired from the Indian National Center for Ocean Information Services (INCOIS) for the period of 01-Jan-2016 to 31-Mar-2016, 01-Jan-2015 to 30-Mar-2016, and 01-Jan-2015 to 31-Mar-2016, respectively. Hourly SST of BoB Deep (BD) ocean Network for Northern Indian (OMNI) moored buoys, BD10 and BD11, are also obtained from the INCOIS for the period of 12-Feb-2017 to 10-Mar-2019 and 01-Jan-2017 to 27-May-2019, respectively [17]. This study uses the RM15 dataset for MHW identification due to its comparatively long-term availability than any other aforementioned in situ dataset (Fig. 1).

B. Methodology

For comparing GHRSST and OISST against in situ data, four nearest neighbors about the site of in situ equipment were averaged. The one or two-day missing data for GHRSST and RM15 has been filled using the linear interpolation method. Outliers have been removed from the WRB data using the median-based outlier detection algorithm present in MATLAB.

To understand the SST variability, comparative wavelet analysis has been performed to highlight the differences in the dominant modes of variability in GHRSST, OISST, and RM15. It is a signal processing technique that decomposes a signal into different frequency components over time [18], [19]. This helps us analyze how the contribution of these components to the total signal varies over time. The wavelet transforms of a 1D-signal (in this case the SST) result in a 2-D pattern of localized power (or variance [20]) in time-frequency space. Relatively higher power of a particular frequency at a specific time indicates a relatively strong presence of that particular frequency component at that time. The patterns outside the Cone of Influence are not considered as they suffer from edge effects [20]. In our study, SST datasets were also filtered for <1, 1–2, and 2–4 months of periodicity range, using the Butterworth-bandpass filter, available in MATLAB.

MHWs are defined as an extreme temperature event where the SST is higher than seasonally varying 90th percentile "threshold" (1) for at least five consecutive days. The discreet heatwave events with a gap of less than 2 days are considered as a single event. Temperatures that are higher than the threshold but do not satisfy the criteria of MHWs are called MHSs [6]. The "threshold" (T_{90}; following [9]) has been defined using the daily climatology (μ) and standard deviation (σ) of SST data computed for the period of 2008–2020 as

$$T_{90} = z \cdot \sigma + \mu \quad (\text{where, } z = 1.282). \tag{1}$$

MHWs have three important attributes, namely, counts—total number of distinct events in a given period of time, duration—total number of days experiencing MHWs conditions in a given period of time, and Daily Intensity (DI)—difference of observed temperature from climatology when MHW or MHS condition is satisfied.

III. Results and Discussion

A. Validation

On comparing GHRSST and OISST with RM15 for 2008–2020, a good correspondence between them is found. A significant ($p < 0.01$) high correlation coefficient (r) of 0.97 (0.96) was found between GHRSST (OISST) and RM15,

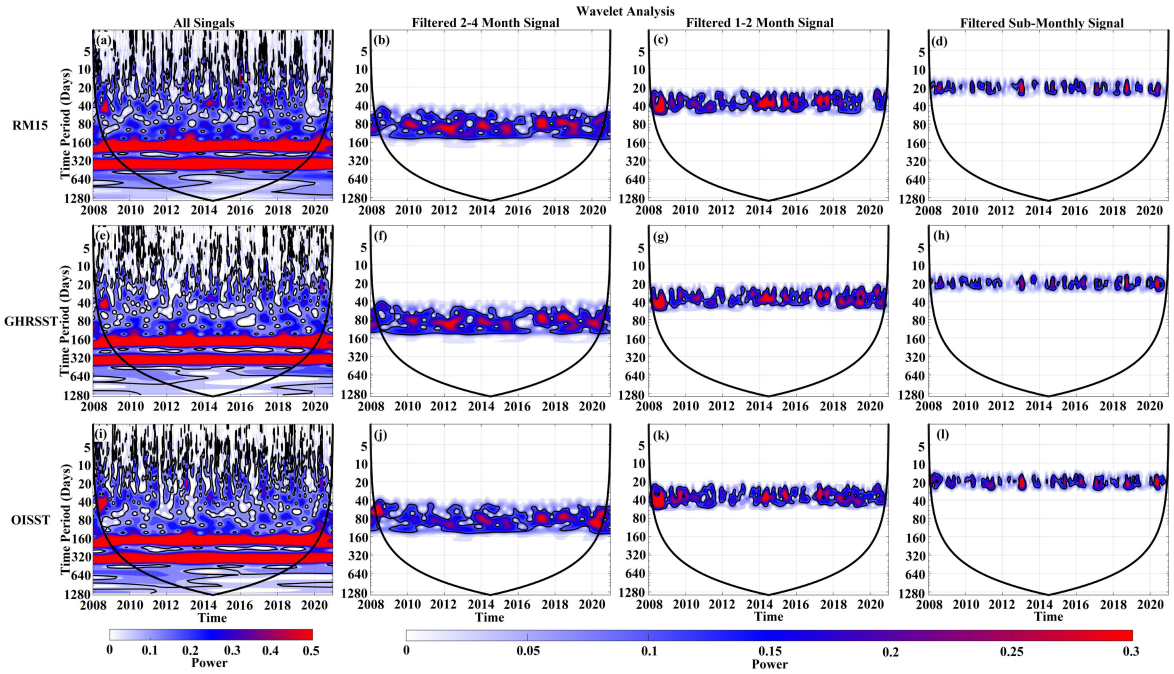

Fig. 3. Wavelet analysis of SST timeseries for (a)–(d) RM15, (e)–(h) GHRSST, and (i)–(l) OISST for all signals, 2–4 months, 1–2 month and sub-monthly scale filtered signals with background representing the power of the signals and solid black curve representing the Cone of Influence.

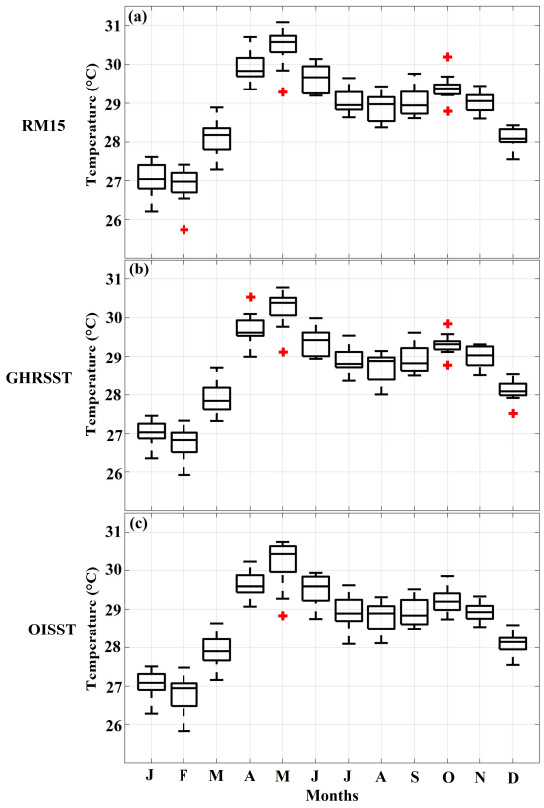

Fig. 4. Box plot of monthly climatology. (a) RM15. (b) GHRSST. (c) OISST.

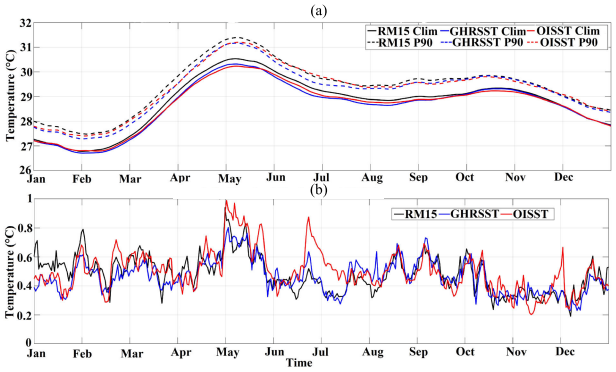

Fig. 5. (a) Timeseries of daily climatology (Clim; solid lines) and 90th percentile threshold (P90; dashed lines) are shown. (b) Time series of daily standard deviation. Black color is used for RM15, red for OISST, and blue for GHRSST.

having a low Root Mean Square Error (RMSE) of 0.30 °C (0.35 °C) [Fig. 2(a)]. The "per decade" trend shown by RM15, GHRSST, and OISST are 0.24 °C, 0.20 °C, and 0.34 °C ($p < 0.01$), respectively. The area-averaged (for the BoB) timeseries of OISST and GHRSST show a high correlation of 0.98 ($p < 0.01$), with an RMSE of 0.20 °C [Fig. 2(b)]. Relatively low correlations and high RMSEs are observed near coastal regions as indicated by WRBD, WRBP, and WRBV against GHRSST and OISST [Fig. 2(c)–(e)]. Again, good correlations and low RMSEs of satellite SST with OMNI buoys (BD10 and BD11) are found [Fig. 2(f) and (g)]. This analysis suggests that GHRSST and OISST perform better in the open ocean compared to coastal regions; therefore, they should be used after proper validation for studying coastal processes.

Wavelet analysis of SST at RM15 [Fig. 3(a)–(d)] are shown in comparison to GHRSST [Fig. 3(e)–(h)] and OISST [Fig. 3(i)–(l)]. For 2–4 month filtered data, GHRSST shows almost a similar pattern as that of RM15 with some underestimation of the power in 2014, whereas OISST deviates both in the pattern and power of the signal, suggesting GHRSST captures processes occurring at a period of 2–4 months more accurately than OISST. For 1–2 months filtered signal, different patterns of dominant signal were observed both in GHRSST and OISST during various years when compared to

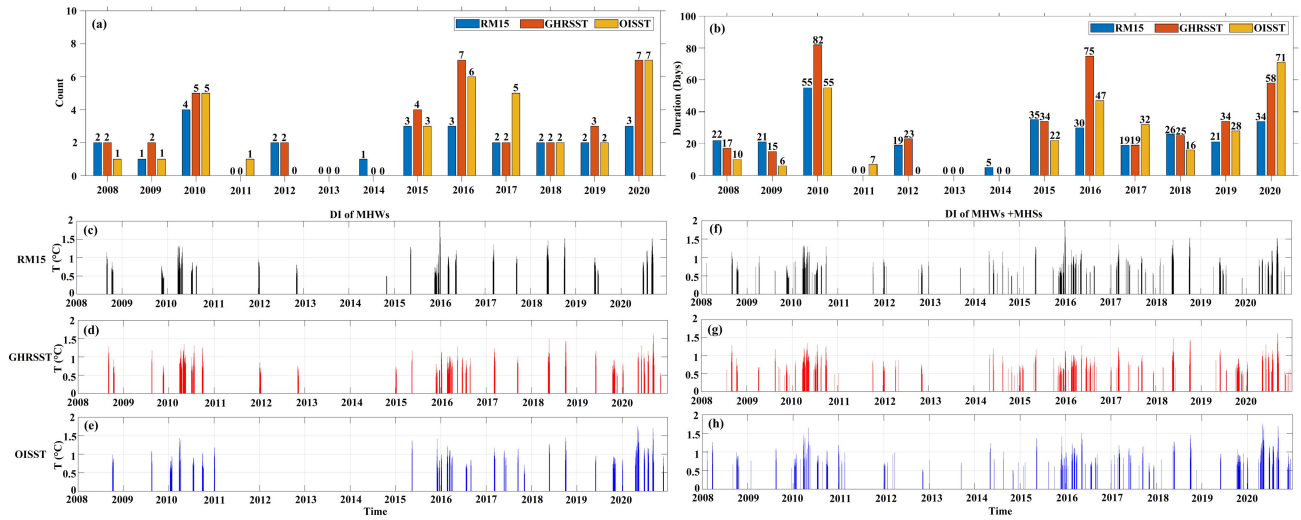

Fig. 6. Bar plot of the number of MHW (a) counts and (b) duration (in days) in a year. Blue bar, red bar, and green bar represent RM15, GHRSST, and OISST respectively. DI of MHWs detected using (c) RM15, (d) GHRSST, and (e) OISST. (f)–(h) are similar to (c)–(e) but for DI of MHWs + MHSs respectively.

RM15, with OISST deviating more than GHRSST. Similarly, in sub-monthly filtered data, GHRSST shows similar patterns as RM15, but OISST is unable to capture it in some of the years. Signals above 2–4 months periodicity are captured by both GHRSST and OISST accurately. Overall, this analysis suggests that GHRSST is more efficient than OISST in capturing signals of different periodicity over the years. Moreover, GHRSST and OISST might show deviations, with respect to RM15, in identifying MHW characteristics owing to their limitation in capturing sub-monthly signals, as MHWs exist for at least 5-days and are primarily driven by sub-monthly processes [9].

B. MHW and MHS Identification

Monthly climatology of OISST has the largest spread about the median followed by RM15 and GHRSST [Fig. 4(a)–(c)], which can also be corroborated by the daily standard deviation [Fig. 5(b)]. To detect the MHW characteristics, it is required to generate daily climatology, standard deviation, and the corresponding threshold [Fig. 5(a) and (b)]. Daily climatology of RM15 is highest followed by OISST and GHRSST; whereas daily threshold of RM15 is highest for almost all the time except for the period of May–July in which the threshold of OISST dominates. This is attributed to the significantly higher values of the standard deviation of OISST compared to RM15, which are used in the calculation of threshold (1).

The MHWs from RM15, GHRSST, and OISST are found to be higher in both counts and duration during the years 2010, 2016, and 2020, albeit with some differences in number. RM15 showed MHW counts and duration of 4 and 55 days, 3 and 30 days, and 3 and 34 days in the aforementioned years, whereas GHRSST (OISST) showed 5 and 82 days (5 and 55 days), 7 and 75 days (6 and 47 days), and 7 and 58 days (7 and 71 days), respectively. Also, these were the years with the most intense MHWs as well [9]. However, OISST in 2020 showed a significantly higher duration of MHWs (71 days) when compared to RM15 (34 days), whereas GHRSST has a duration (58 days) lying between the OISST and RM15. On the other hand, GHRSST showed higher duration in the years 2010 and 2016 when compared to both RM15 and OISST. Additionally, the years 2011, 2013, and 2014 showed inconspicuous or zero MHW events which are more or less consistent with all the datasets. In the year 2012, both GHRSST and RM15 showed an equal number of counts (two), and similar duration (19 days and 23 days respectively), whereas OISST showed no heatwave event. After 2014, all years have experienced frequent and intense MHWs which is also consistent with Gupta et al. [9].

The yearly statistics of MHWs characteristics from satellite products showed overestimation in counts and duration when compared to RM15 [Fig. 6(a) and (e)]. In contrast, the DI has similar values whenever the MHWs were captured by all three datasets [Fig. 6(b)–(d)]. The total count and duration of MHWs using RM15 were found to be 25 and 287 days respectively for the study period. In contrast, GHRSST (OISST) overestimates both count and duration with a total of 36 (33) and 382 (294) days respectively. Owing to the values above, the average duration per count comes out to be 11.48 days, 10.61 days, and 8.91 days for the RM15, GHRSST, and OISST respectively. The statistically significant ($p < 0.01$) correlation of the counts and duration between the RM15 and GHRSST (OISST) were 0.85 (0.74) and 0.88 (0.74) respectively. The mean DI from RM15, GHRSST, and OISST were similar with a value of 0.87 °C, 0.82 °C, and 0.90 °C, respectively. The correlations ($p < 0.01$) of the DI of RM15 against GHRSST and OISST were observed to be 0.72 and 0.57, respectively.

To understand the source of the overestimation of MHW count and duration by GHRSST and OISST compared to RM15, MHSs have been plotted with MHWs [Fig. 6(f)–(h)]. It was found that the duration (DI) of MHWs and MHSs when taken together are 418 days (0.84 °C), 490 days (0.79 °C), and 413 days (0.88 °C) for RM15, GHRSST, and OISST respectively, suggesting a reduced difference in MHW + MHS duration. Therefore, the discrepancy in MHW count and duration comes from the fact that these MHSs do not persist longer than 5-days to be categorized as MHWs at RM15,

whereas in GHRSST and OISST, there is sustenance of MHSs for a longer duration resulting in more MHWs.

IV. Conclusion

This study assesses the applicability of GHRSST and OISST datasets in identifying MHWs in comparison to moored buoy observations in the BoB. A good agreement between the satellite-derived SST and in situ SST has been found to hold in the open ocean region (maximum RMSE of 0.36 °C across all in situ measurements). However, GHRSST and OISST showed higher RMSEs when compared to WRBs present near the coastal regions (minimum RMSE of 0.51 °C across all the WRB locations), and therefore, GHRSST and OISST datasets are not good estimates of in situ temperatures near the coastal region. Hence, they should be used after extensive validation for studying coastal processes. Consequently, these satellite datasets are suggested to be improved with respect to capturing coastal SST variabilities. Moreover, GHRSST and OISST are unable to capture the signals having periodicity <2 months with the same power and frequency as that of RM15; however, GHRSST captures 2–4 months signals more accurately. Wavelet analysis suggested that GHRSST is better than OISST in capturing signals with different frequencies. Moreover, monthly and daily climatology and daily standard deviations for GHRSST, OISST, and RM15 were slightly different from one another resulting in differing 90th percentile thresholds calculated for these datasets. MHWs, which are becoming more frequent and hazardous to aquatic life in the BoB [9], are also being overestimated by GHRSST (count $=$ 36 and duration $=$ 382 days) and OISST (count $=$ 33 and duration $=$ 294 days) due to sustenance of high temperature for longer period than RM15 (count $=$ 25 and duration $=$ 287 days). However, the duration of MHWs and MHSs taken together shows a better match in all the cases showing the efficacy of GHRSST and OISST in detecting heat extremes.

This study showed the applicability of the OISST and GHRSST in accurately identifying the MHS and MHW characteristics in the BoB. Therefore, these datasets can be utilized for understanding the spatial distribution of MHWs along with their formation and dissipation mechanism. This analysis also motivates us to investigate the reasons for the recent increment in the long-sustained MHW events in the region. In addition, the results can further be utilized for validation of any model-simulated SSTs in this region. Furthermore, there is a scope to look into the vertical extension of MHWs in this region using observations or models.

Acknowledgment

The authors would like to thank IIT Bhubaneswar for infrastructural support. They would like to thank Rahul Deogharia from IIT Bhubaneswar for scientific discussions. Authors acknowledge the editors and reviewers for constructive suggestions.

References

[1] Y. Kawai and A. Wada, "Diurnal sea surface temperature variation and its impact on the atmosphere and ocean: A review," *J. Oceanogr.*, vol. 63, no. 5, pp. 721–744, Oct. 2007.

[2] M. Roxy et al., "A reduction in marine primary productivity driven by rapid warming over the tropical Indian Ocean," *Geophys. Res. Lett.*, vol. 43, no. 2, pp. 826–833, 2016.

[3] Y. Duan, H. Zhang, Y. Gao, and M. Zhou, "Efficient extraction of coastal upwelling in the northern South China sea based on sea surface temperature data and research of its interannual variations," *IEEE Geosci. Remote Sens. Lett.*, vol. 20, 2023, Art. no. 1501205.

[4] S. Dey and S. Sil, "Spatio-temporal variability of coastal upwelling using high resolution remote sensing observations in the bay of Bengal," *Estuarine, Coastal Shelf Sci.*, vol. 282, Mar. 2023, Art. no. 108228.

[5] A. Fahad, B. Singh, M. Kamal, T. Ahmed, M. Kibria, and N. Chowdhury, "The role of local topography and sea surface temperature on summer monsoon precipitation over Bangladesh and northeast India," *Int. J. Climatol.*, vol. 42, no. 9, pp. 4564–4579, 2022.

[6] A. Hobday et al., "A hierarchical approach to defining marine heatwaves," *Prog. Oceanogr.*, vol. 141, pp. 227–238, Feb. 2016.

[7] J. Saranya, M. Roxy, P. Dasgupta, and A. Anand, "Genesis and trends in marine heatwaves over the tropical Indian Ocean and their interaction with the Indian summer monsoon," *J. Geophys. Res., Oceans*, vol. 127, no. 2, 2022, Art. no. e2021JC017427.

[8] S. Rathore, R. Goyal, B. Jangir, C. Ummenhofer, M. Feng, and M. Mishra, "Interactions between a marine heatwave and tropical cyclone amphan in the Bay of Bengal in 2020," *Frontiers Climate*, vol. 4, Jun. 2022, Art. no. 861477.

[9] H. Gupta, S. Sil, A. Gangopadhyay, and G. Gawarkiewicz, "Observed surface and subsurface Marine Heat Waves in the Bay of Bengal from in-situ and high-resolution satellite data," *Climate Dyn.*, vol. 62, pp. 203–221, Aug. 2024.

[10] Y. Cheng et al., "A quantitative analysis of marine heatwaves in response to rising sea surface temperature," *Sci. Total Environ.*, vol. 881, Jul. 2023, Art. no. 163396.

[11] K. Kilpatrick, G. Podesta, and R. Evans, "Overview of the NOAA/NASA advanced very high resolution radiometer Pathfinder algorithm for sea surface temperature and associated matchup database," *J. Geophys. Res., Oceans*, vol. 106, pp. 9179–9197, May 2001.

[12] Y. Wang, C. Wu, and S. Chao, "Warming and weakening trends of the Kuroshio during 1993–2013," *Geophys. Res. Lett.*, vol. 43, pp. 9200–9207, Sep. 2016.

[13] F. Al Senafi, "Atmosphere-ocean coupled variability in the Arabian/Persian Gulf," *Frontiers Mar. Sci.*, vol. 9, Feb. 2022, Art. no. 809355.

[14] X. Ren and W. Liu, "The role of a weakened Atlantic meridional overturning circulation in modulating marine heatwaves in a warming climate," *Geophys. Res. Lett.*, vol. 48, no. 23, 2021, Art. no. e2021GL095941.

[15] Z. Huang, M. Feng, H. Beggs, S. Wijffels, M. Cahill, and C. Griffin, "High-resolution marine heatwave mapping in Australasian waters using Himawari-8 SST and SSTAARS data," *Remote Sens. Environ.*, vol. 267, Dec. 2021, Art. no. 112742.

[16] M. Mcphaden et al., "RAMA: The research moored array for African–Asian–Australian monsoon analysis and prediction," *Bull. Amer. Meteorol. Soc.*, vol. 90, no. 4, pp. 459–480, Apr. 2009.

[17] R. Venkatesan et al., "In situ ocean subsurface time-series measurements from OMNI buoy network in the Bay of Bengal," *Current Sci.*, vol. 104, no. 9, pp. 1166–1177, 2013.

[18] A. Graps, "An introduction to wavelets," *IEEE Comput. Sci. Eng.*, vol. 2, no. 2, pp. 50–61, Summer 1995.

[19] C. Torrence and G. P. Compo, "A practical guide to wavelet analysis," *Bull. Amer. Meteorol. Soc.*, vol. 79, no. 1, pp. 61–78, Jan. 1998.

[20] L. Aguiar-Conraria, N. Azevedo, and M. J. Soares, "Using wavelets to decompose the time–frequency effects of monetary policy," *Phys. A, Stat. Mech. Appl.*, vol. 387, no. 12, pp. 2863–2878, May 2008.